Chemical Science

ROYAL SOCIETY OF CHEMISTRY

EDGE ARTICLE

View Article Online
View Journal | View Issue

Open Access Article. Published on 08 February 2022. Downloaded on 2/8/2026 4:57:08 AM.
This article is licensed under a Creative Commons Attribution-NonCommercial 3.0 Unported Licence.

Check for updates

Cite this: *Chem. Sci.*, 2022, **13**, 2692

All publication charges for this article have been paid for by the Royal Society of Chemistry

Palladium-catalyzed selective C–C bond cleavage and stereoselective alkenylation between cyclopropanol and 1,3-diyne: one-step synthesis of diverse conjugated enynes†

Bedadyuti Vedvyas Pati, Asit Ghosh, Komal Yadav, Shyam Kumar Banjare, Shalini Pandey, Upakarasamy Lourderaj * and Ponneri C. Ravikumar *

Received 30th August 2021
Accepted 24th January 2022

DOI: 10.1039/d1sc04780a

rsc.li/chemical-science

The stereoselective synthesis of 1,3-enynes from 1,3-diynes is demonstrated by palladium-catalyzed selective C–C bond cleavage of cyclopropanol. Exclusive formation of mono-alkenylated adducts was achieved by eliminating the possibility of di-functionalization with high stereoselectivity. Indeed, this protocol worked very well with electronically and sterically diverse substrates. Several studies, including deuterium labeling experiments and intermolecular competitive experiments, were carried out to understand the mechanistic details. The atomic-level mechanism followed in the catalytic process was also validated using DFT calculations, and the rate-controlling states in the catalytic cycle were identified. Furthermore, preliminary mechanistic investigations with radical scavengers revealed the non-involvement of the radical pathway in this transformation.

Introduction

Transition metal-catalysed selective cleavage of C–H and C–C bonds has gained enormous significance in recent years owing to its potential application in chemical transformations.[1,2] Especially, the strategy involving selective cleavage of a C–H bond followed by subsequent insertion of a 2π-unsaturated unit has been recognized as one of the most attractive approaches to access diverse molecular entities from the readily available feedstock.[3] This strategy also helps in building rapid complexity following the high atom-economical process. In this context, the one-step synthesis of conjugated 1,3-enynes through this process is of great importance due to their vast abundance in various natural products and pharmaceuticals (Scheme 1).[4]

Consequently, they have been well recognized as multifaceted building units in organic synthesis.[5] Moreover, these structural units also received considerable interest in materials science and medicinal chemistry.[6]

Considering their profound synthetic usefulness, 1,3-diynes have been recently introduced as a coupling partner for transition-metal catalysed reactions to access conjugated 1,3-enynes.[7] Nevertheless, the use of 1,3-diynes in these reactions is always associated with particular challenges. The most commonly faced challenges are: (a) difficulty in controlling stereo- and regio-selectivity and (b) difficulty in controlling mono-functionalization over di-functionalization.[3b,7] As a result, only a few protocols for the synthesis of 1,3-enynes using 1,3-diynes have been described to date.[7] Ge and co-workers developed a cobalt-catalysed regiodivergent and stereoselective hydroboration of 1,3-diynes to afford boryl-functionalized enynes (Scheme 2a(i)).[7a] In another report, Beller and co-workers also disclosed palladium-catalysed selective synthesis of conjugated enynes employing alkoxycarbonylation of 1,3-diynes (Scheme 2a(ii)).[7b] Interestingly, highly selective synthesis of 1,3-enynes was also achieved by Glorius and co-workers *via*

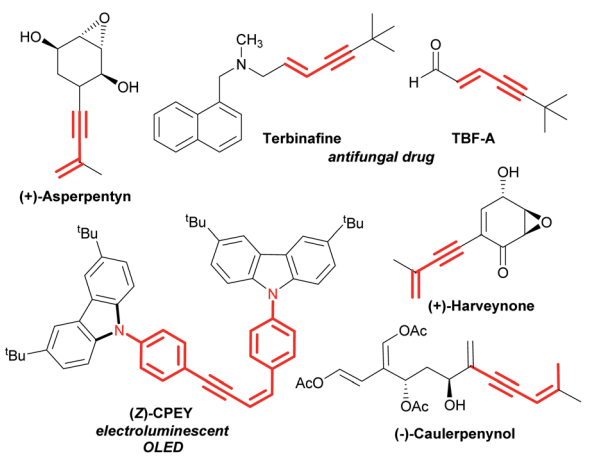

Scheme 1 Representative examples of natural products and drug molecules bearing conjugated 1,3-enyne scaffolds.

School of Chemical Sciences, National Institute of Science Education and Research (NISER) Bhubaneswar, HBNI, Jatani, Khurda, 752050 Odisha, India. E-mail: u.lourderaj@niser.ac.in; pcr@niser.ac.in

† Electronic supplementary information (ESI) available. See DOI: 10.1039/d1sc04780a

© 2022 The Author(s). Published by the Royal Society of Chemistry

Open Access Article. Published on 08 February 2022. Downloaded on 2/8/2026 4:57:08 AM.
This article is licensed under a Creative Commons Attribution-NonCommercial 3.0 Unported Licence.

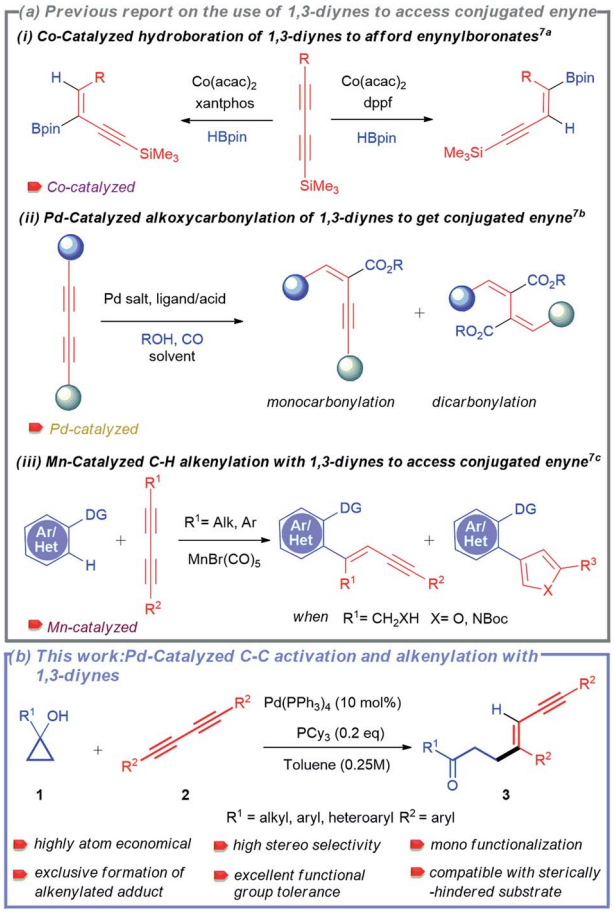

Scheme 2 Use of 1,3-diynes to access conjugated enynes. (a) Previous report and (b) this work.

manganese-catalysed C–H activation-alkenylation of arenes and heteroarenes with 1,3-diynes (Scheme 2a(iii)).[7c] Because of the challenges mentioned above, reports on using 1,3-diynes to synthesize conjugated enynes are minimal. Although palladium-catalysed hydroalkylation of alkynes with cyclopropanols was developed by Yao and co-workers,[11h] the possibility of selective C–C bond cleavage and alkenylation sequence for 1,3-dynes has never been attempted.

In this context, the tandem cleavage and functionalization of the C–C bond is quite challenging. It is mainly owing to the thermodynamic stability and kinetic inertness of C–C bonds. In addition, poor accessibility and poor orbital directionality of C–C bonds by the catalyst as compared to C–H bonds make them less favorable for effective interactions with transition metal complexes. Despite these difficulties, substantial efforts have been made over the last two decades to functionalize different types of C–C bonds.[2,8] Some valuable strategies employed include β-carbon elimination,[8a,c] oxidative addition,[2d] and aromatization driven processes.[8d] In this regard, one of the recent and attractive processes includes the cleavage of the C–C bond of small rings by taking advantage of their intrinsic ring strain.[9] The thermodynamic barrier is largely offset with the aid of release of ring strain. The synthetic potential of this method was successfully demonstrated by several research groups such as the Dong, Jun, Murakami, Bower, Yu, Loh, and Marek groups to access an array of useful structural motifs.[10] Cyclopropanol obtained from Kulinkovich protocol is one of the smallest ring molecules whose ring strain has been exploited to synthesize various molecular architectures utilizing metal-homoenolates.[11–13] Our group has also developed the strain-driven C–C bond cleavage of cyclopropanol and cyclopropenone to furnish diverse functionalized molecular units.[14]

Owing to the synthetic value of conjugated enynes and the significance of developing new methodology using 1,3-diynes, we envisioned that the strain-driven C–C bond cleavage-subsequent alkenylation of cyclopropanol would effectively result in the formation of the desired 1,3-enynes. Herein, we report a palladium-catalysed selective C–C bond cleavage and stereo-selective mono-alkenylation of readily accessible cyclopropanol to rapidly synthesize divergent 1,3-enynes (Scheme 2b).

Results and discussion

To establish our methodology, we started by identifying the suitable reaction conditions for the palladium-catalysed C–C bond activation of cyclopropanol and the subsequent alkenylation with 1,3-diyne. Subsequently, 1-benzylcyclopropan-1-ol **1a** and 1,4-diphenylbuta-1,3-diyne **2a** were chosen as the model substrates in the presence of 10 mol% of a palladium catalyst. Initially, different palladium catalysts were screened in the absence of a ligand in toluene at 100 °C (Table 1, entries 1–5). The desired alkenylated adduct **3aa** was obtained in 19% and 56% yields with $Pd(dba)_2$ and $Pd(PPh_3)_4$ respectively (Table 1, entries 3 and 5). Other palladium catalysts such as $PdCl_2$, $PdCl_2(PPh_3)_2$, and $Pd(OCOCF_3)_2$ remained ineffective (Table 1, entries 1, 2 and 4). The use of other solvents such as tetrahydrofuran, acetonitrile, and dimethylformamide, with $Pd(PPh_3)_4$ as the catalyst, did not improve the product yield (Table 1, entries 6–8). Increasing or decreasing the reaction temperature (120 °C and 80 °C) had a deleterious effect on the reaction furnishing the desired product **3aa** in 34% and 42% yields, respectively (Table 1, entries 9 and 10). Hence, we chose $Pd(PPh_3)_4$ as the catalyst in toluene at 100 °C and varied the other reaction parameters. It is worth mentioning here that the reactive metal-homoenolate generated after the β-carbon elimination from **1a** may undergo protodemetalation and β-hydride elimination to give a ring-opened isomerized product and α,β-unsaturated ketone respectively resulting in a significant loss of the product yield. Therefore, we increased the equivalence of **1a**. To our delight, 69% of **3aa** was obtained using 2 equivalents of **1a** (Table 1, entry 11). Next, we investigated the effects of different electron-rich *N*-heterocyclic and phosphine ligands (Table 1, entries 12–20). No improvement in the yield of **3aa** was noticed using electron-rich *N*-heterocyclic ligands (Table 1, entries 12–15). Gratifyingly, product yield was further enhanced in the cases of $P(^tBu)_3.HBF_4$ (77%) and PCy_3 (89%) (Table 1, entries 18, 19). However, a reduced yield of **3aa** was observed with the PCy_3-$Pd(PPh_3)_4$ catalyst at lower temperatures (Table 1, entries 21 and 22). Furthermore, varying the molar percentage

Open Access Article. Published on 08 February 2022. Downloaded on 2/8/2026 4:57:08 AM.
This article is licensed under a Creative Commons Attribution-NonCommercial 3.0 Unported Licence.

Table 1 Optimization of reaction conditions[a]

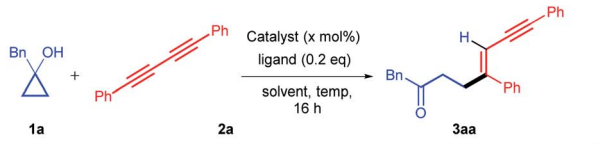

Entry	Catalyst	Ligand	Solvent	Temp (°C)	Yield[b]
1	$PdCl_2$	-	Toluene	100	nd[c]
2	$PdCl_2(PPh_3)_2$	-	Toluene	100	nd[c]
3	$Pd(dba)_2$	-	Toluene	100	19
4	$Pd(OCOCF_3)_2$	-	Toluene	100	nd[c]
5	$Pd(PPh_3)_4$	-	Toluene	100	56
6	$Pd(PPh_3)_4$	-	THF	100	40
7	$Pd(PPh_3)_4$	-	MeCN	100	29
8	$Pd(PPh_3)_4$	-	DMF	100	25
9	$Pd(PPh_3)_4$	-	Toluene	80	34
10	$Pd(PPh_3)_4$	-	Toluene	120	42
11[d]	$Pd(PPh_3)_4$	-	Toluene	100	69
12[d]	$Pd(PPh_3)_4$	IMes·HCl	Toluene	100	52
13[d]	$Pd(PPh_3)_4$	IPr·HCl	Toluene	100	16
14[d]	$Pd(PPh_3)_4$	ICy·HBF_4	Toluene	100	38
15[d]	$Pd(PPh_3)_4$	L[e]	Toluene	100	27
16[d]	$Pd(PPh_3)_4$	PPh_3	Toluene	100	53
17[d]	$Pd(PPh_3)_4$	RuPhos	Toluene	100	62
18[d]	$Pd(PPh_3)_4$	$P(^tBu)_3.HBF_4$	Toluene	100	77
19[d]	**$Pd(PPh_3)_4$**	**PCy_3**	**Toluene**	**100**	**89(86)**
20[d]	$Pd(PPh_3)_4$	$PCy_3.HBF_4$	Toluene	100	68
21[d]	$Pd(PPh_3)_4$	PCy_3	Toluene	60	56
22[d]	$Pd(PPh_3)_4$	PCy_3	Toluene	80	63
23[d,f]	$Pd(PPh_3)_4$	PCy_3	Toluene	100	73
24[d,g]	$Pd(PPh_3)_4$	PCy_3	Toluene	100	77
25[d]	-	PCy_3	Toluene	100	nd[c]

[a] Unless otherwise specified, all reactions were carried out using catalyst (10 mol%), ligand (0.2 equiv.), **1a** (0.10 mmol, 1.0 equiv.), and **2a** (0.10 mmol, 1.0 equiv.) in a solvent (0.25 M) for 16 h. [b] Yields determined by NMR, using 1,3,5-trimethoxy benzene as the internal reference. [c] nd = not detected. [d] Using **1a** (0.20 mmol, 2.0 equiv.) and **2a** (0.10 mmol, 1.0 equiv.) while the other conditions remained the same. [e] L = 3-(*tert*-butyl)-1-(2,6-diisopropylphenyl)-1*H*-imidazol-3-ium hexafluorophosphate (V). [f] Using a catalyst (5 mol%) while the other conditions remained the same. [g] Using catalyst (10 mol%) and ligand (0.1 equiv.) while the other conditions remained the same. Isolated yield is mentioned in the parenthesis.

of $Pd(PPh_3)_4$ and PCy_3 did not increase the product yield (Table 1, entries 23 and 24). We then performed a control experiment without the $Pd(PPh_3)_4$ catalyst. As expected, it did not produce the product, thus, confirming the key role of the catalyst in this reaction (entry 25). Hence, the use of 10 mol% of $Pd(PPh_3)_4$, 0.2 equivalents of PCy_3 in toluene (0.25 M) at 100 °C is the best optimized condition for the synthesis of **3aa** (Table 1, entry 19).

Having established the optimized reaction conditions, we next moved to assess the robustness of this highly stereoselective alkenylation of cyclopropanols (Table 2). To showcase the diversity of this protocol, we subjected various benzyl-, alkyl-, aryl-, heteroaryl-substituted cyclopropanols **1** and aryl-substituted 1,3-diynes **2** to the standard reaction conditions. Initially, we examined the feasibility of different benzyl-

Table 2 Scope of cyclopropanols for the synthesis of conjugated enynes[a]

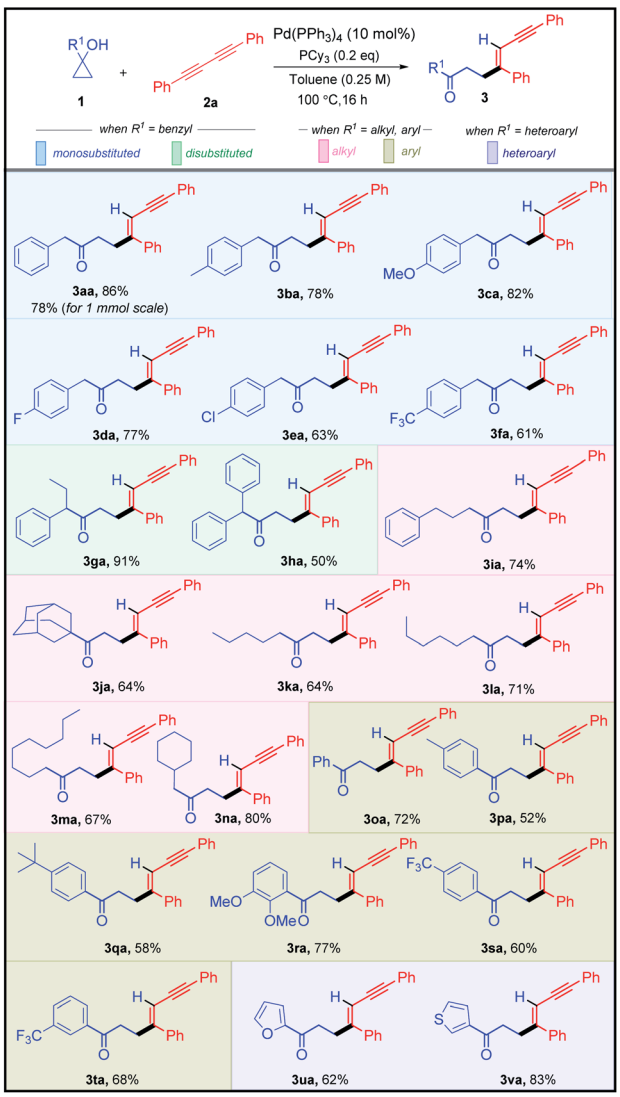

[a] All reactions were carried out using $Pd(PPh_3)_4$ (10 mol%), PCy_3 (0.2 equiv.), **1** (0.20 mmol, 2.0 equiv.), and **2a** (0.10 mmol, 1.0 equiv.) in toluene (0.25 M) at 100 °C for 16 h.

© 2022 The Author(s). Published by the Royal Society of Chemistry

Open Access Article. Published on 08 February 2022. Downloaded on 2/8/2026 4:57:08 AM.
This article is licensed under a Creative Commons Attribution-NonCommercial 3.0 Unported Licence.

substituted cyclopropanols. Cyclopropanols bearing Me, OMe, F, Cl, and CF_3 substituents worked efficiently, furnishing 61–86% yield of their respective alkenylated adducts **3aa–3fa**. Furthermore, we also found that the alkenylation reaction was viable with disubstituted cyclopropanols affording their respective adducts **3ga** and **3ha** in 91% and 50% yields respectively. It is worth mentioning that various alkyl (linear-chain and alicyclic) substituted cyclopropanols and sterically hindered cyclopropanol **1j** reacted smoothly to produce the desired alkenylated adducts **3ia–3na** in 64–80% yield.

After successfully demonstrating the scope of alkenylation with benzyl- and alkyl-substituted cyclopropanols, we focused our attention on unraveling the scope of different aryl- and heteroaryl-substituted cyclopropanols. Similar to the benzyl-substituted cyclopropanols, Me, ^{t}Bu, 2,3-di-OMe, and CF_3 substituted aryl cyclopropanols were facile, resulting in good yields of their corresponding alkenylated adducts **3oa–3ta**. Pleasingly, cyclopropanols bearing furan- and thiophene-substituents underwent the transformation efficiently, yielding **3ua** and **3va** in 62% and 83% yield, respectively.

After successfully exploring the scope of structurally and electronically distinct cyclopropanols for the developed methodology, we further investigated the scope with different 1,3-diynes (Table 3). Both electronically rich and poor 1,3-diynes furnished their corresponding alkenylated adducts **3ab–3aj** in 61–94% yields. The regio- and the stereo-selectivity of the product molecule was confirmed unambiguously from the NOE experiment of **3aa**. To test the synthetic practicality of the developed C–C activation protocol, we performed a 1 mmol scale reaction with **1a** and **2a** to produce **3aa** in 78% yield.

Encouraged by the versatility of the developed transformation, we performed a series of experiments to get insight into the mechanism of the catalytic cycle. Initially, we

Table 3 Scope of 1,3-diynes for the synthesis of conjugated enynes[a]

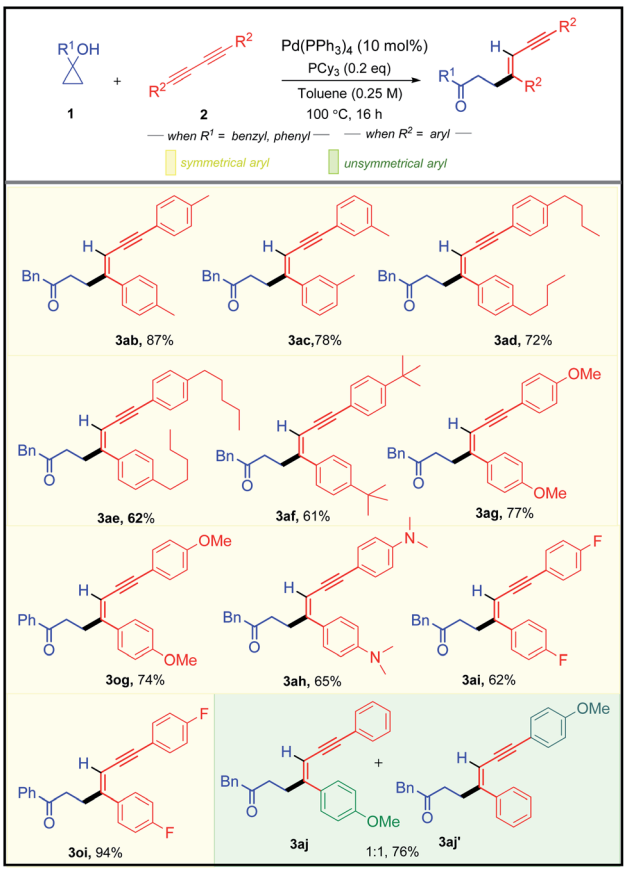

[a] All reactions were carried out using $Pd(PPh_3)_4$ (10 mol%), PCy_3 (0.2 equiv.), **1** (0.20 mmol, 2.0 equiv.), and **2a** (0.10 mmol, 1.0 equiv.) in toluene (0.25 M) at 100 °C for 16 h.

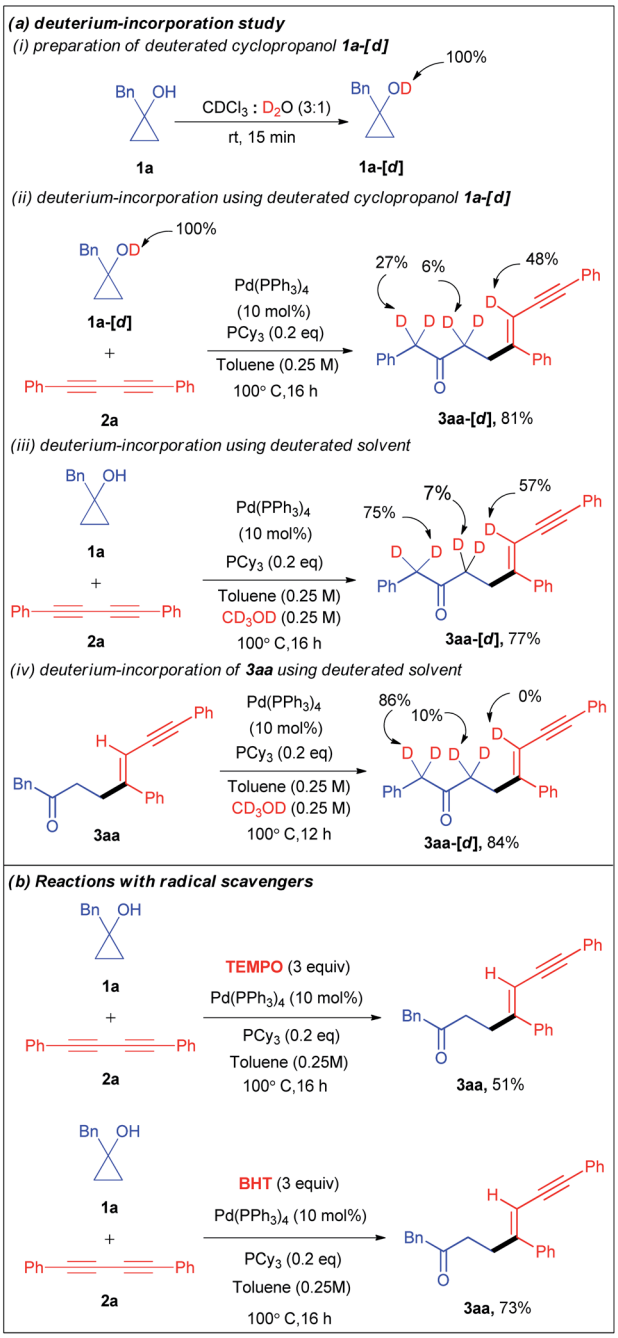

Scheme 3 Mechanistic studies.

Open Access Article. Published on 08 February 2022. Downloaded on 2/8/2026 4:57:08 AM.
This article is licensed under a Creative Commons Attribution-NonCommercial 3.0 Unported Licence.

conducted a set of deuterium incorporation studies using the deuterated substrate **1a-[*d*]** and deuterated solvent CD_3OD (Scheme 3a). The reaction of **1a-[d]** (100% D) and **2a** afforded **3aa-[d]** in 81% yield with 48% deuteration at the olefinic proton, 6% deuteration at the carbonyl α-position and 27% deuteration at the benzylic proton of **3aa-[d]** (Scheme 3aii). When we used CD_3OD as a co-solvent, 57% deuteration at the olefinic proton, 75% deuteration at the benzylic proton, and 7% deuteration at the carbonyl α-position of **3aa-[d]** were observed with 77% yield (Scheme 3aiii). These results reveal that not only the alcoholic protons but also the carbonyl α-protons are also the proton source for the olefinic position. Furthermore, the treatment of the isolated product **3aa** with CD_3OD under the optimized conditions resulted in no deuteration at the olefinic position of **3aa-[d]** (Scheme 3aiv). To investigate the involvement of a radical pathway, we carried out two reactions in the presence of radical scavengers such as 2,2,6,6-tetramethylpiperidine 1-oxyl (TEMPO) and 2,6-di-*tert*-butyl-4-methyl-phenol (BHT) (Scheme 3b). The **3aa** yields of 51% and 73% in the presence of TEMPO and BHT respectively refuted the possibility of a radical pathway.

Moreover, for further mechanistic insights and to understand the electronic effects, we conducted two intermolecular competitive experiments. First, a one pot competition reaction between two electronically different aryl cyclopropanols **1p** and **1s** was performed under the standard reaction conditions with diyne **2a**, affording **3pa** : **3sa** in a 6.14 : 1 ratio (see ESI section 4.1.1-page S16† for details). In a similar vein, the competition reaction between the cyclopropanols in a parallel set of reactions resulted in **3pa** : **3sa** in a 3.3 : 1 ratio (Scheme 4a). Similarly, another set of one pot competition reactions between two different cyclopropanols **1b** and **1f** (benzyl substituents) when reacted with diyne **2a**, produced **3ba** : **3fa** in a 1 : 0.90 ratio (see ESI section 4.1.3-page S21† for details). Clearly, these experimental observations indicate the role of direct relay of electronic effects in the aryl substrates which are absent in the benzyl substrates. Next, the one pot competitive experiment between two different diynes **2g** and **2i** with cyclopropanol **1a** afforded **3ag** : **3ai** in a 1 : 1.68 ratio (see ESI section 4.2.1-page S23† for details). Similarly, the competitive one pot reaction between diynes **2g** and **2i** with cyclopropanol **1o** le to **3og** : **3oi** in a 1 : 2.16 ratio (see ESI section 4.2.2-page S25† for details). Likewise, the competition reaction between the diynes **2g** and **2i** with cyclopropanol **1o** in a parallel set of reactions resulted in **3og** : **3oi** in a 1 : 1.2 (Scheme 4a). These results reveal that alkenylation is more favourable for electronically rich cyclopropanols and electronically poor diynes.

To gain insight into the atomic-level mechanism followed in the reaction between **1a** and **2a** catalyzed by $Pd(PPh_3)_4$, we performed density functional theory (DFT) calculations using the B3LYP-D3 (ref. 15–17) functional with 6-31G(d,p)[18] basis sets and the SDD[19] and LANL2DZ[20] pseudopotentials to represent the core electrons of Pd. The LANL2DZ and SDD pseudopotentials have successfully been used in several studies to represent the core electrons of Pd.[21,22] We performed all calculations in the presence of toluene as the solvent using the SMD[23] solvation model and mapped the (Gibbs) free energy profiles

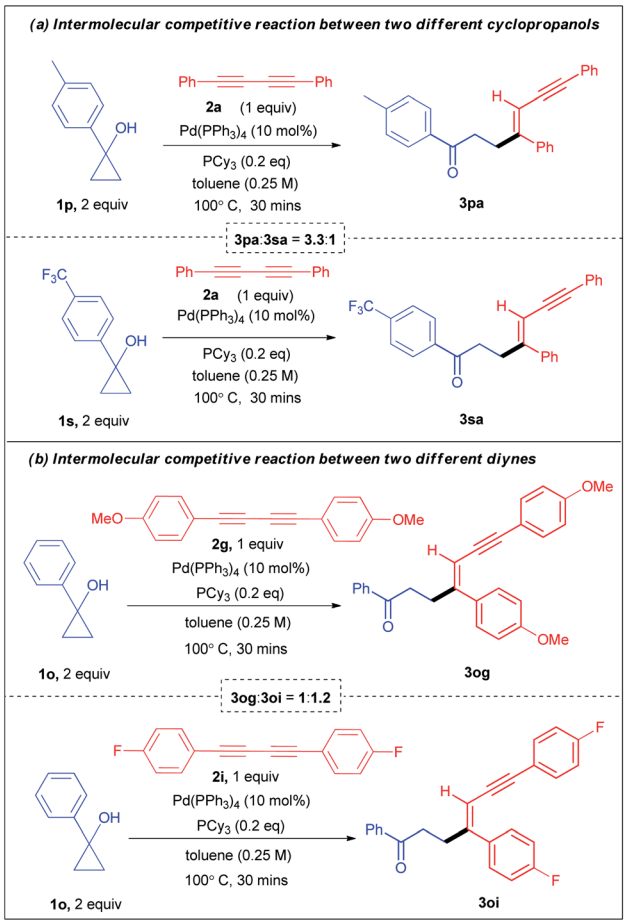

Scheme 4 Competitive experiments.

along the reaction paths. The free energies were calculated by considering different pathways at the experimental temperature of 373.15 K. See the ESI† for a detailed description of the methods and the different reaction pathways considered in the DFT study. We found that the overall nature of the reaction profiles for different pathways was similar when using the SDD and LANL2DZ pseudopotentials. However, the SDD gave comparatively lower barriers for the various pathways considered and hence we discuss below the mechanisms obtained using the B3LYP-D3/6-31G(d,p)/SDD level of theory.

In cross-coupling reactions involving Pd catalysts, PdL_4 dissociates to PdL_3, which is in equilibrium with PdL_2.[24] PdL_2 has been observed to behave as the active species and thus controls the oxidative addition step. The energy of the active species, PdL_2 was found to be 6.4 kcal mol^{-1} lower as compared to that of PdL_4, where L = PPh_3. The relative energies were computed with respect to PdL_4. Due to the complexity of the reaction, we considered different types of mechanisms for the catalytic cycle. Four different pathways were investigated: (i) Path I: oxidative addition → 1,3-diyne coordination → β-carbon elimination → *syn*-addition → reductive elimination (Fig. 1 and Scheme 5), (ii) Path II: 1,3-diyne coordination → ligand exchange with cyclopropanol → *syn*-addition → β-carbon elimination → reductive elimination (Fig. S3 and S4†),

© 2022 The Author(s). Published by the Royal Society of Chemistry

Open Access Article. Published on 08 February 2022. Downloaded on 2/8/2026 4:57:08 AM.
This article is licensed under a Creative Commons Attribution-NonCommercial 3.0 Unported Licence.

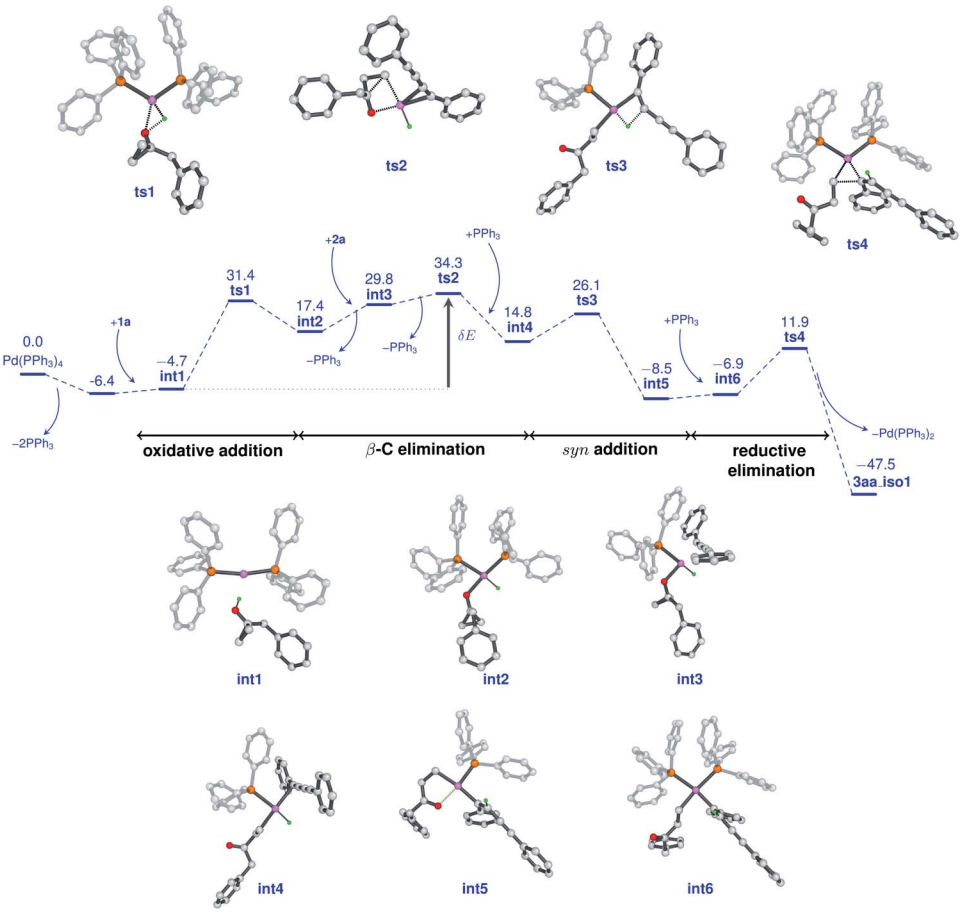

Fig. 1 Free energy profile for the reaction between **1a** and **2a** catalyzed by **Pd(PPh3)4**, calculated at the B3LYP-D3/6-31G(d,p)/SDD level of theory. The energies are reported in kcal mol^{-1}. The effective free energy barrier (δ*E*) for the reaction is shown by the dark gray arrow.

(iii) Path III: oxidative addition → β-carbon elimination → 1,3-diyne coordination → *syn*-addition → reductive elimination (Fig. S5 and S6†), and (iv) Path IV: oxidative addition → 1,3-diyne coordination → *syn*-addition → β-carbon elimination → reductive elimination (Fig. S7 and S8†). The effective barriers calculated using the energy span model[25] for Paths I–IV were 39.0, 49.1, 36.1, and 43.9 kcal mol^{-1} respectively indicating that Path III could be the favorable mechanism with oxidative addition as the rate-determining step. However, the deuterium substituted reaction resulted in a KIE value of 1.70 (refer to the ESI† for details). This KIE value was found to be in sharp contrast to the theoretically calculated KIE (3.77, refer to the ESI† for details) computed by considering the oxidative addition barrier of 36.1 kcal mol^{-1} for Path III. These observations clearly revealed the non-involvement of the O–H oxidative-addition as the rate-limiting-step and hence Path III was eliminated as the possible reaction pathway. Moreover, the electronic effect seen in Scheme 4 cannot be explained if O–H activation is the rate-limiting step (Path III). Of the remaining three reaction pathways considered, Path I had the lowest effective barrier and was found to be consistent with the experimental observations as discussed below. Fig. 1 gives the complete free energy profile for the reaction path (Path I) involving various stationary points. The molecular structures and important geometrical parameters of the stationary points are given in Fig. S1 and S9 in the ESI.† The catalytic reaction cycle begins with the approach of the active catalyst $Pd(PPh_3)_2$ and **1a** towards each other to form the complex **int1** having an energy of −4.7 kcal mol^{-1} with the H atom of the OH group of **1a** pointing towards Pd (H–Pd distance = 2.28 Å). The next step is the oxidative addition of the alcoholic –OH group[11f,g] to the Pd center to result in **int2**. The oxidative addition is achieved by the concerted dissociation of the O–H bond and the formation of Pd–O and Pd–H coordinate bonds *via* a three-membered cyclic transition state **ts1** with a barrier of 36.1 kcal mol^{-1} with respect to **int1**. In **int2**, the Pd center is tetracoordinated with Pd–O (2.06 Å) and Pd–H (1.57 Å) bonds and has a square planar geometry. Then, the addition of **2a** to palladium takes place to result in **int3** preceded by the elimination of PPh_3 which is crucial to lower the steric hindrance and accommodate incoming **2a**. It should be noted that the free rotation of the O–C bond in the intermediates (**int1** and **int2**) leads to the formation of different conformational isomers. However, the energy differences between the conformational isomers were less than 1 kcal mol^{-1}. The intermediate **int3** then undergoes β-carbon elimination to form **int4**. During this process, a PPh_3 group is first eliminated to give **int3′**. Then,

Open Access Article. Published on 08 February 2022. Downloaded on 2/8/2026 4:57:08 AM.
This article is licensed under a Creative Commons Attribution-NonCommercial 3.0 Unported Licence.

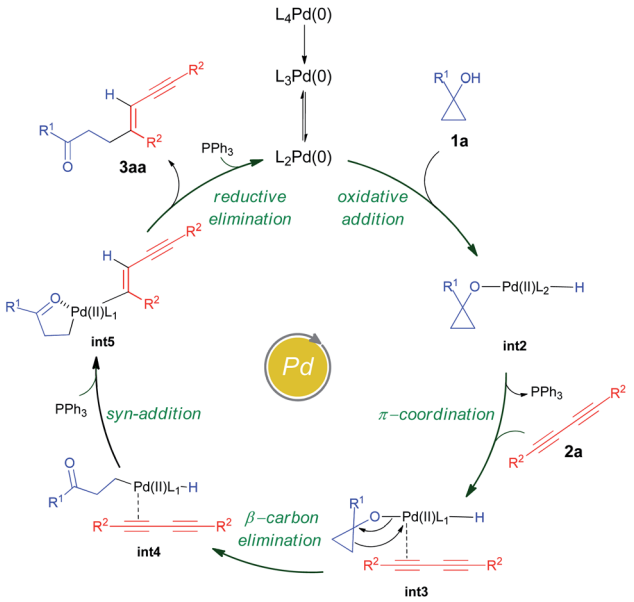

Scheme 5 Proposed catalytic cycle.

the Pd–C_β bond is formed which is accompanied by the simultaneous breaking of the C_α–C_β and O–Pd bonds *via* a four-membered cyclic transition state **ts2** with a barrier of 4.5 kcal mol^{-1} with respect to **int3** to form **int3″**. A PPh_3 group is then added to **int3″** to give **int4**. The intermediates **int3′** and **int3″**are not shown in Fig. 1 for clarity. What ensues is the hydrogenation of the unsaturated alkyne bond by the *syn* addition of Pd–H to the C≡C bond to form the intermediate **int5**. This is a concerted step *via* a four-membered cyclic transition state **ts3** with a barrier of 11.3 kcal mol^{-1}. When going from **int4** to **ts3**, the hydrogen atom of the Pd–H bond is stretched, and the C≡C bond is aligned coplanar to the square planar orientation of the Pd center to facilitate the H···C≡C interaction. From **ts3**, the H migration results in **int5** with the Pd center maintaining a planar geometry.

Now, the addition of a PPh_3 group to **int5** leads to the formation of the intermediate **int6** with a *tetra*-coordinated Pd center. The final step in the cycle is the reductive elimination process at the Pd center from **int6** to the product **3aa_iso1**. Here, the two Pd–C bonds in **int6** are broken with the concomitant bond formation between the associated carbon atoms *via* a cyclic three-membered transition state **ts4** with a 18.8 kcal mol^{-1} barrier. The product **3aa_iso1** is stabilized by −47.5 kcal mol^{-1} with respect to the reactants. The product **3aa_iso1** can exist in different isomeric forms (**3aa_iso2**, **3aa_iso3**, and **3aa_iso4**, Fig. S2†) due to rotation about C–C sigma bonds that are within 4 kcal mol^{-1} in energies.

It is of interest to identify the rate-controlling states involved in the overall reaction. To this end, we computed the turnover frequency (TOF) for the reaction using the energetic span model.[25] From the energetics of the reaction, we can see that the TOF determining transition state (TDTS) and the TOF determining intermediate (TDI) are **ts2** and **int1**, respectively. Hence, the effective free energy barrier (δE) for the catalytic cycle is 39.0 kcal mol^{-1} which is lower than that of the **Paths II** and **IV**, as noted in the energy profile (Fig. 1).

It should be noted that the competitive experiments (Scheme 4a) of the electron rich and poor cyclopropanols with diynes (**2a**) resulted in a ratio of 3.3 : 1 (**3pa** : **3sa**). Moreover, reactions of the electron rich (**2g**) and poor (**2i**) diynes with cyclopropanol (**1**) resulted in a ratio of 1 : 1.2 (**3og** : **3oi**). To understand this distribution in the products where electron rich cyclopropanols and electron poor diynes are favoured, we calculated the thermal rate constants using the Eyring-Polanyi equation[26,27] at 373.15 K. For the reactions involving *p*-Me-cyclopropanol and *p*-CF_3-cyclopropanol, the k_{TST}(**3pa**)/k_{TST}(**3sa**) was found to be 2.3 : 1, whereas the k_{TST}(**3og**)/k_{TST}(**3oi**) was found to be 1 : 1.42, in close agreement with the experimentally observed product ratios. In addition, the KIE (k_H/k_D) calculated from the DFT free energies of 2.56 was found to be in qualitative agreement with the experimentally determined value of 1.70, indicating the absence of any primary kinetic isotope effect in the reaction. Thus, the agreement of the calculated KIE and product ratios from the DFT energies with the experimental KIE and product ratios obtained in the electronic effect experiments, further supports Path I as the possible mechanism.

In accordance with the aforementioned mechanistic outcomes from the experiments supported by the DFT calculations at the B3LYP-D3/6-31G(d,p)/SDD level of theory and literature precedents,[11] a plausible catalytic cycle is depicted in Scheme 5. The catalytic cycle starts with the oxidative addition of cyclopropanol[11f,g] **1a** to the active $PdL_2(0)$ catalyst to form the intermediate **int2**. The intermediate **int2** then undergoes π-coordination with 1,3-diyne **2a** to afford the intermediate **int3**. β-Carbon elimination from **int3** leads to the formation of the intermediate **int4.** This intermediate **int4** then undergoes *syn* addition with hydrogen atom transfer to furnish the homoenolate intermediate **int5**. Finally, the reductive elimination of palladium homoenolate intermediate **int5** results in the alkenylated adduct **3aa** with the regeneration of the Pd(0) catalyst.

Conclusions

In conclusion, we have developed a palladium-catalyzed novel and highly stereo-selective synthetic strategy to get an array of 1,3-enyne derivatives *via* selective C–C bond cleavage of cyclopropanol followed by alkenylation with 1,3-diynes. Apart from high and stereo-selectivity, excellent functional group tolerance has also been achieved with both cyclopropanol and 1,3-diynes. The protocol was found to be amenable to sterically hindered cyclopropanols such as adamantane cyclopropanol. Importantly, by eliminating the possibility of difunctionalization, exclusive mono-functionalization has also been achieved. Several mechanistic investigations including deuterium labelling experiments have been carried out. In addition, the reaction mechanism of the catalytic process was supported using DFT calculations and it was found that the step corresponding to the ring opening of cyclopropanol acted as the rate-controlling step for the reaction. The preliminary mechanistic findings with radical scavengers revealed non-involvement of the radical pathway in the transformation.

© 2022 The Author(s). Published by the Royal Society of Chemistry

Open Access Article. Published on 08 February 2022. Downloaded on 2/8/2026 4:57:08 AM. This article is licensed under a Creative Commons Attribution-NonCommercial 3.0 Unported Licence.

Data availability

We have deposited all the experimental and computational data as ESI.†

Author contributions

B. V. P. planned, conducted, and analyzed the experiments, and A. G. carried out the substrate scope and contributed in writing the first draft of the manuscript. S. K. B. carried out the mechanistic studies. K. Y. conducted the computational studies. S. P. carried out the NOE experiments. P. C. R. supervised the overall project and U. L. supervised the computational calculations in the project. All authors contributed to discussions and commented on the manuscript.

Conflicts of interest

There are no conflicts to declare.

Dedication

This work is dedicated to Prof. S. Chandrasekaran, IISc, Bangalore, on the occasion of his 75th birthday.

Acknowledgements

We acknowledge DAE, Govt. of India, Council of Scientific and Industrial Research (CSIR), New Delhi (Grant 02(0256)/16/EMR II), and the Science and Engineering Research Board (SERB), New Delhi (Grant EMRII/2017/001475) for financial support. B. V. P. thanks DST-INSPIRE, and A. G., K. Y., S. K. B., and S. P. thank the DAE for the research fellowship.

Notes and references

1 For selected recent reviews on transition-metal-catalyzed C−H activation, see: (*a*) J. Wencel-Delord and F. Glorius, *Nat. Chem.*, 2013, **5**, 369–375; (*b*) G. Rouquet and N. Chatani, *Angew. Chem., Int. Ed.*, 2013, **52**, 11726–11743; (*c*) V. S. Thirunavukkarasu, S. I. Kozhushkov and L. Ackermann, *Chem. Commun.*, 2014, **50**, 29–39; (*d*) M. Moselage, J. Li and L. Ackermann, *ACS Catal.*, 2016, **6**, 498–525; (*e*) J. R. Hummel, J. A. Boerth and J. A. Ellman, *Chem. Rev.*, 2017, **117**, 9163–9227; (*f*) C. Sambiagio, D. Schonbauer, R. Blieck, T. Dao-Huy, G. Pototschnig, P. Schaaf, T. Wiesinger, M. F. Zia, J. Wencel-Delord, T. Besset, B. U. W. Maesa and M. Schnürch, *Chem. Soc. Rev.*, 2018, **47**, 6603–6743; (*g*) P. Gandeepan, T. Müller, D. Zell, G. Cera, S. Warratzand and L. Ackermann, *Chem. Rev.*, 2019, **119**, 2192–2452; (*h*) U. Dutta, S. Maiti, T. Bhattacharya and D. Maity, *Science*, 2021, **372**, 701 and references cited therein.

2 For selected recent reviews on transition-metal-catalyzed C−C activation, see: (*a*) M. Murakami and T. Matsuda, *Chem. Commun.*, 2011, **47**, 1100–1105; (*b*) K. Ruhland, *Eur. J. Org. Chem.*, 2012, 2683–2706; (*c*) F. Chen, T. Wang and N. Jiao, *Chem. Rev.*, 2014, **114**, 8613–8661; (*d*) L. Souillart and N. Cramer, *Chem. Rev.*, 2015, **115**, 9410–9464; (*e*) M. Murakami and N. Ishida, *J. Am. Chem. Soc.*, 2016, **138**, 13759–13769; (*f*) P.-h. Chen, B. A. Billett, T. Tsukamoto and G. Dong, *ACS Catal.*, 2017, **7**, 1340–1360; (*g*) F. Song, T. Gou, B.-Q. Wang and Z.-J. Shi, *Chem. Soc. Rev.*, 2018, **47**, 7078–7115; (*h*) T. R. McDonald, L. R. Mills, M. S. West and S. A. L. Rousseaux, *Chem. Rev.*, 2021, **121**, 3–79 and references cited therein.

3 For selected examples, see: (*a*) W. Zhang, H. Li and L. Wang, *Adv. Synth. Catal.*, 2019, **361**, 2885–2896; (*b*) D.-G. Yu, F. de Azambuja, T. Gensch, C. G. Daniliuc and F. Glorius, *Angew. Chem., Int. Ed.*, 2014, **53**, 9650–9654; (*c*) S. Kathiravan and I. Nicholls, *Org. Lett.*, 2017, **19**, 4758–4761; (*d*) M. S. R. Mandal, A. Das, D. Kalsi and B. Sundararaju, *Chem.–Eur. J.*, 2017, **23**, 17454–17457; (*e*) Y. Gao, F. F. Zeng, X. D. Sun, M. F. Zeng, Z. Yang, X. Q. Huang, G. D. Shen, Y. S. Tan, R. K. Feng and C. Z. Qi, *Adv. Synth. Catal.*, 2018, **360**, 1328–1333; (*f*) Á. M. Martínez, I. Alonso, N. Rodríguez, R. G. Arrayás and J. C. Carretero, *Chem.–Eur. J.*, 2019, **25**, 5733–5742; (*g*) R. Feng, H. Ning, H. Su, Y. Gao, H. Yin, Y. Wang, Z. Yang and C. Qi, *J. Org. Chem.*, 2017, **82**, 10408–10417; (*h*) R. Mei, W. Ma, Y. Zhang, X. Guo and L. Ackermann, *Org. Lett.*, 2019, **21**, 6534–6538; (*i*) S. Kumar, A. M. Nair and C. M. R. Volla, *Org. Lett.*, 2020, **22**, 2141–2146; (*j*) A. Dey and C. M. R. Volla, *Org. Lett.*, 2020, **22**, 7480–7485; (*k*) B. V. Pati, P. S. Sagara, A. Ghosh, G. K. D. Adhikari and P. C. Ravikumar, *J. Org. Chem.*, 2021, **82**, 10408–10417; (*l*) F. Zhao, X. Gong, Y. Lu, J. Qiao, X. Jia, H. Ni, X. Wu and X. Zhang, *Org. Lett.*, 2021, **23**, 727–733.

4 For selected examples, see: (*a*) A. Rudi, M. Schleyer and Y. Kashman, *J. Nat. Prod.*, 2000, **63**, 1434–1436; (*b*) S. L. Iverson and J. P. Uetrecht, *Chem. Res. Toxicol.*, 2001, **14**, 175–181; (*c*) N. El-Jaber, A. Estévez-Braun, A. G. Ravelo, O. Munoz-Munoz, A. Rodrí-guez Afonso and J. R. Murguia, *J. Nat. Prod.*, 2003, **66**, 722–724; (*d*) A. Fürstner and L. Turet, *Angew. Chem., Int. Ed.*, 2005, **44**, 3462–3466.

5 For selected reviews, see: (*a*) R. G. Bergman, *Acc. Chem. Res.*, 1973, **6**, 25–31; (*b*) S. Saito and Y. Yamamoto, *Chem. Rev.*, 2000, **100**, 2901–2916; (*c*) R. Chinchilla and C. Njera, *Chem. Rev.*, 2014, **114**, 1783–1826; (*d*) M. Holmes, L. A. Schwartz and M. J. Krische, *Chem. Rev.*, 2018, **118**, 6026–6052; (*e*) Y. Xiao and J. Zhang, *Angew. Chem., Int. Ed.*, 2008, **47**, 1903–1906; (*f*) D. J. Burns, D. Best, M. D. Wieczysty and H. W. Lam, *Angew. Chem., Int. Ed.*, 2015, **54**, 9958–9962; (*g*) Y. Huang, J. del Pozo, S. Torker and A. H. Hoveyda, *J. Am. Chem. Soc.*, 2018, **140**, 2643–2655; (*h*) C. Ye, Y. Li, X. Zhu, S. Hu, D. Yuan and H. Bao, *Chem. Sci.*, 2019, **10**, 3632–3636; (*i*) X. Zhu, W. Deng, M.-F. Chiou, C. Ye, W. Jian, Y. Zeng, Y. Jiao, L. Ge, Y. Li, X. Zhang and H. Bao, *J. Am. Chem. Soc.*, 2019, **141**, 548–559.

6 For selected examples, see: (*a*) C.-K. Choi, I. Tomita and T. Endo, *Macromolecules*, 2000, **33**, 1487–1488; (*b*) K. Campbell, C. J. Kuehl, M. J. Ferguson, P. J. Stang and R. R. Tykwinski, *J. Am. Chem. Soc.*, 2002, **124**, 7266–7267; (*c*) Y. Liu, M. Nishiura, Y. Wang and Z. Hou, *J. Am. Chem. Soc.*, 2006, **128**, 5592–5593; (*d*) G. S. Pilzak, K. van

Open Access Article. Published on 08 February 2022. Downloaded on 2/8/2026 4:57:08 AM. This article is licensed under a Creative Commons Attribution-NonCommercial 3.0 Unported Licence.

Gruijthuijsen, R. H. van Doorn, B. van Lagen, E. J. R. Sudhçlter and H. Zuilhof, *Chem.–Eur. J.*, 2008, **14**, 7939–7950; (*e*) Z. Cao and T. Ren, *Organometallics*, 2011, **30**, 245–250.

7 For selected examples, see: (*a*) H. L. Sang, C. Wu, G. G. D. Phua and S. Ge, *ACS Catal.*, 2019, **9**, 10109–10114; (*b*) J. Liu, J. Yang, C. Schneider, R. Frank, R. Jackstell and M. Beller, *Angew. Chem., Int. Ed.*, 2020, **59**, 9032–9040; (*c*) S. Cembellín, T. Dalton, T. Pinkert, F. Schäfers and F. Glorius, *ACS Catal.*, 2020, **10**, 197–202; (*d*) J. Liu, C. Schneider, J. Yang, Z. Wei, H. Jiao, R. Franke, R. Jackstell and M. Beller, *Angew. Chem., Int. Ed.*, 2021, **133**, 375–383; (*e*) F. Sun, C. Yang, J. Ni, G. J. Cheng and X. Fang, *Org. Lett.*, 2021, **23**, 4045–4050.

8 For selected examples, see: (*a*) A. Korotvička, I. Císařová, J. Roithová and M. Kotora, *Chem.–Eur. J.*, 2012, **18**, 4200–4207; (*b*) Z. Gu, G. B. Boursalian, V. Gandon, R. Padilla, H. Shen, T. V. Timofeeva, P. Tongwa, K. P. C. Vollhardt and A. A. Yakovenko, *Angew. Chem., Int. Ed.*, 2011, **50**, 9413–9417; (*c*) H. Takano, K. S. Kanyiva and T. Shibata, *Org. Lett.*, 2016, **18**, 1860–1863; (*d*) Y. Xu, X. Qi, P. Zheng, C. C. Berti, P. Liu and G. Dong, *Nature*, 2019, **567**, 373–378 and references cited therein.

9 (*a*) G. Fumagalli, S. Stanton and J. F. Bower, *Chem. Rev.*, 2017, **117**, 9404–9432; (*b*) B. Biletskyi, P. Colonna, K. Mason, J. L. Parrain, L. Commeiras and G. Chouraqui, *Chem. Soc. Rev.*, 2021, **50**, 7513–7538.

10 For selected examples, see: (*a*) C.-H. Jun, H. Lee, C. W. Moon and H.-S. Hong, *J. Am. Chem. Soc.*, 2001, **123**, 8600–8601; (*b*) L. Jiao, C. Yuan and Z.-X. Yu, *J. Am. Chem. Soc.*, 2008, **130**, 4421–4430; (*c*) L. Deng, M. Chen and G. Dong, *J. Am. Chem. Soc.*, 2018, **140**, 9652–9658; (*d*) J. Bruffaerts, A. Vasseur, S. Singh, A. Masarwa, D. Didier, L. Oskar, L. Perrin, O. Eisenstein and I. Marek, *J. Org. Chem.*, 2018, **83**, 3497–3515; (*e*) X. Ma, I. R. Hazelden, T. Langer, R. H. Munday and J. F. Bower, *J. Am. Chem. Soc.*, 2019, **141**, 3356–3360; (*f*) S. Li, P. Shi, R.-H. Liu, X.-H. Hu and T.-P. Loh, *Org. Lett.*, 2019, **21**, 1602–1606.

11 For selected examples, see: (*a*) D. Rosa and A. Orellana, *Chem. Commun.*, 2013, **49**, 5420–5422; (*b*) B. B. Parida, P. P. Das, M. Niocel and J. K. Cha, *Org. Lett.*, 2013, **15**, 1780–1783; (*c*) K. Cheng and P. J. Walsh, *Org. Lett.*, 2013, **15**, 2298–2301; (*d*) N. Nithiy and A. Orellana, *Org. Lett.*, 2014, **16**, 5854–5857; (*e*) A. Reding, P. G. Jones and D. B. Werz, *Org. Lett.*, 2018, **20**, 7266–7269; (*f*) J. Le. Bras and J. Muzart, *Tetrahedron*, 2019, **76**(12), 130879, DOI: 10.1016/j.tet.2019.130879; (*g*) H. Okumoto, T. Jinnai, H. Shimizu, Y. Harada, H. Mishima and A. Suzuki, *Synlett*, 2000, 629–630; (*h*) H. Liu, Z. Fu, S. Gao, Y. Huang, A. Lin and H. Yao, *Adv. Synth. Catal.*, 2018, **360**, 3171–3175.

12 For selected examples, see: (*a*) Z. Ye and M. Dai, *Org. Lett.*, 2015, **17**, 2190–2193; (*b*) Z. Ye, K. E. Gettys, X. Shen and M. Dai, *Org. Lett.*, 2015, **17**, 6074–6077; (*c*) Y. Li, Z. Ye, T. M. Bellman, T. Chi and M. Dai, *Org. Lett.*, 2015, **17**, 2186–2189; (*d*) X.-P. He, Y.-J. Shu, J.-J. Dai, W.-M. Zhang, Y.-S. Feng and H.-J. Xu, *Org. Biomol. Chem.*, 2015, **13**, 7159–7163; (*e*) H. Zhang, G. Wu, H. Yi, T. Sun, B. Wang, Y. Zhang, G. Dong and J. Wang, *Angew. Chem., Int. Ed.*, 2017, **56**, 3945–3950; (*f*) Y. A. Konik, M. Kudrjashova, N. Konrad, S. Kaabel, I. Järving, M. Lopp and D. G. Kananovich, *Org. Biomol. Chem.*, 2017, **15**, 8334–8340; (*g*) Z. Ye, X. Cai, J. Li and M. Dai, *ACS Catal.*, 2018, **8**, 5907–5914; (*h*) E. Gyanchander, S. Ydhyam, N. Tumma, K. Belmore and J. K. Cha, *Org. Lett.*, 2016, **18**, 6098–6101 and references cited therein.

13 For selected examples, see: (*a*) J. Yang, Y. Shen, Y. J. Lim and N. Yoshikai, *Chem. Sci.*, 2018, **9**, 6928–6934; (*b*) J. Yang, Q. Sun and N. Yoshikai, *ACS Catal.*, 2019, **9**, 1973–1978; (*c*) J. Yang, Y. Sekiguchi and N. Yoshikai, *ACS Catal.*, 2019, **9**, 5638–5644; (*d*) L. R. Mills, C. H. Zhou, E. Fung and S. A. L. Rousseaux, *Org. Lett.*, 2019, **21**, 8805–8809; (*e*) J. Li, Y. Zheng, M. Huang and W. Li, *Org. Lett.*, 2020, **22**, 5020–5024; (*f*) Y. Sekiguchi and N. Yoshikai, *J. Am. Chem. Soc.*, 2021, **143**(12), 4775–4781; (*g*) W. Huang and F. Meng, *Angew. Chem., Int. Ed.*, 2021, **60**, 2694–2698.

14 For selected examples, see: (*a*) T. Nanda and P. C. Ravikumar, *Org. Lett.*, 2020, **22**, 1368–1374; (*b*) B. V. Pati, A. Ghosh and P. C. Ravikumar, *Org. Lett.*, 2020, **22**, 2854–2860; (*c*) T. Nanda, P. Biswal, B. V. Pati, S. K. Banjare and P. C. Ravikumar, *J. Org. Chem.*, 2021, **86**(3), 2682–2695.

15 C. Lee, W. Yang and R. G. Parr, *Phys. Rev. B: Condens. Matter Mater. Phys.*, 1988, **37**, 785–789.

16 A. D. Becke, *J. Chem. Phys.*, 1993, **98**, 1372–1377.

17 S. Grimme, J. Antony, S. Ehrlich and H. Krieg, *J. Chem. Phys.*, 2010, **132**, 154104.

18 T. Clark, J. Chandrasekhar, G. W. Spitznagel and P. V. R. Schleyer, *J. Comput. Chem.*, 1983, **4**, 294–301.

19 P. Fuentealba, H. Stoll, L. Von Szentpaly, P. Schwerdtfeger and H. Preuss, *J. Phys. B Atom. Mol. Phys.*, 1983, **16**, 323–328.

20 W. R. Wadt and P. J. Hay, *J. Chem. Phys.*, 1985, **82**(1), 284–298.

21 S. Bag, A. Mondal, R. Jayarajan, U. Dutta, S. Porey, R. B. Sunoj and D. Maiti, *J. Am. Chem. Soc.*, 2020, **142**(28), 12453–12466.

22 F. Proutiere and F. Schoenebeck, *Angew. Chem., Int. Ed.*, 2011, **50**(35), 8192–8195.

23 A. V. Marenich, C. J. Cramer and D. G. Truhlar, *J. Phys. Chem. B*, 2009, **113**, 6378–6396.

24 U. W. Maes, S. Verbeeck, T. Verhelst, A. Ekomié, N. von Wolff, G. Lefèvre, E. A. Mitchell and A. Jutand, *Chem.–Eur. J.*, 2015, **21**, 7858–7865.

25 S. Kozuch, *Wiley Interdiscip. Rev.: Comput. Mol. Sci.*, 2012, **2**, 795–815.

26 H. Eyring, *J. Chem. Phys.*, 1935, **3**(2), 107–115.

27 H. Eyring and M. Polanyi, *Z. Phys. Chem., Abt. B*, 1931, **12**, 279–311.

© 2022 The Author(s). Published by the Royal Society of Chemistry